

Characterization of Candle Flames

ANTHONY HAMINS* AND MATTHEW BUNDY
*National Institute of Standards and Technology
Gaithersburg, MD 20899-8663, USA*

SCOTT E. DILLON
*Bureau of Alcohol, Tobacco and Firearms – Fire Research Lab
Ammendale, MD 20705, USA*

ABSTRACT: Common household open flame and radiant ignition sources are the actual or suspected cause for many fires. The purpose of this research is to identify the burning behavior and properties of common candles in order to provide additional tools for use by fire investigators. The properties of paraffin wax are obtained from the literature and from experiments. The candles are burned under controlled laboratory conditions to measure the mass burning rate, candle regression rate, flame height, and heat flux. Using the properties of paraffin wax and characteristics of the candles, numerous simulations are performed with the NIST Fire Dynamics Simulator (FDS) to model the burning rate and heat flux profile of the candle flame. The modeling results are then compared with the flame height and heat flux data obtained experimentally. The model facilitates an enhanced understanding of the structure of candle flames.

KEY WORDS: arson, candles, fire model, flames, ignition, paraffin, wax.

INTRODUCTION

THE USE OF candles in the US has been increasing annually since the early 1990s. According to the National Candle Association (NCA), candles are used in 7 out of 10 homes, and retail candle sales exceed approximately \$2.3 billion annually with a growth rate exceeding 15% [1]. The increased use of candles has resulted in a corresponding increase in the number of candle-related fires. In 1998, the US Consumer Product Safety

*Author to whom correspondence should be addressed. E-mail: anthony.hamins@nist.gov

Commission (CPSC) estimated that there were 12,800 candle-related fires that resulted in 170 deaths and 1200 injuries [2]. In 2001, the National Fire Protection Association (NFPA) estimated that candles were responsible for approximately 18,000 residential structural fires, which caused 190 civilian fatalities, \$265 M in property loss, and 1500 civilian injuries [3]. Candles account for a large proportion of the injuries from all residential fires [4]. A 2002 study reported that unattended candles are the number one cause of candle-related fires, closely followed by candles placed in close proximity to combustible materials [5]. The types of materials most often ignited by candles were found to be mattresses or bedding, cabinetry, and curtains and blinds or drapery. Forty-five percent of candle-related fires were found to originate in the bedroom [5]. Despite the rise in candle use and candle-related fires, very little information is available to fire investigators to establish the likelihood of a candle being the cause of a fire.

Faraday gave the first comprehensive scientific study on the physics of candle burning almost 150 years ago [6]. Through a series of simple and elegant experiments, exceptional insight was provided on the chemical structure and fluid mechanics associated with the combustion of candle burning. Almost all recent studies on the structure of small laminar non-premixed flames have focused on more controlled combustion situations, involving for example, slot burner flames or flames involving reactants flowing through co-annular tubes. This study reverts to the examination of actual candles, with the purpose of characterizing candle flames to support the work of fire investigators, who need quantitative information on possible sources of fire ignition. This study involves the characterization of burning candles including their mass burning rate, heat release rate, regression rate, flame height, wick length and shape, and the heat flux profile about the flame. Data on the thermophysical properties of candle wax was reviewed to better describe the energetics of candle burning. The properties of the wax and the physical dimensions of a burning candle were used as input for a computational model that was developed to simulate a burning candle flame. The candle flame model was favorably compared with experimental results, allowing an enhanced understanding of the structure of candle flames.

OVERVIEW OF CANDLES

A modern candle consists primarily of wax and a wick. The wax can be mixed or formulated with additives such as dyes or pigments for color, fragrances for scent, as well as other ingredients that affect the surface finish and adhesion. The most common type of wax used in the candle making

process is petroleum-derived paraffin, which has been refined to contain a low percentage of residual oil. The melting point of the paraffin wax used is determined by the manufacturer based on the candle's intended size, shape, and use. Other specialty candles can be made from beeswax, stearic acid, and clear gels. The various dyes and fragrances added to the wax are designed not to interfere with the burning of the candles and to produce 'clean' combustion products (water and carbon dioxide). The actual effects of these additives, however, is unclear. The wick consists of a braided or twisted fabric (usually cotton) that is designed to match the type of candle and wax. The most common type of wick is the flat braid wick, with others being a square or cored braid [7].

The National Candle Association provides the following general descriptions of candles [7]:

- Taper – a slender candle, typically 0.15–0.45 m in height, to be held securely upright by a candle holder (see Figure 1).
- Votive – a small cylindrical candle, usually about 40 mm in diameter and 50 mm or 60 mm high, which is placed in a 'cup' (usually made of glass) to hold the liquefied wax that results from burning; originally produced as white unscented candles for religious ceremonies; they are now available in many colors and scents.
- Pillar or Column – a rigid, self-standing candle that is thick in diameter, with one or more wicks.
- Luminaria – an outdoor candle created by planting a 15-h votive in a container filled with sand.

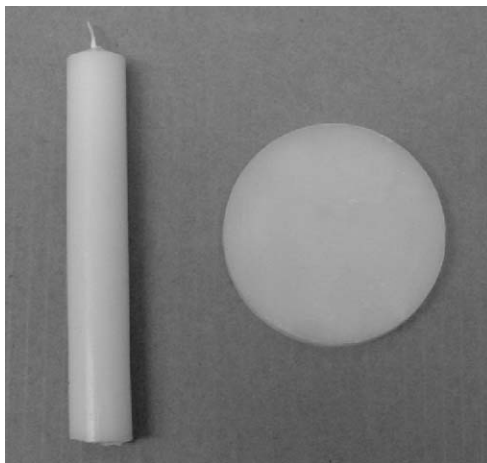


Figure 1. Paraffin wax candle and cone calorimeter test specimen.

- Container or Wax-filled – a candle that is poured into a special glass, tin, or pottery container.
- Tealight – a small cylindrical candle, usually about 25 mm in diameter and 40 mm high, which is filled in its own holder, typically made of metal.
- Specialty – an unusually shaped or sculpted free-standing candle.
- Gel – a transparent-type candle typically having a rubber-like consistency, made primarily from gelled mineral oils or gelled synthetic hydrocarbons, and poured into a container to maintain its shape.
- Floating – a shallow candle with a smooth, slightly convex bottom designed specifically to float on water.

Owing to the various candle types and wax combinations available, the preliminary portion of this study was to focus on a single type of candle. According to the NCA, there are over 350 manufacturers of candles in the US, and a major manufacturer can offer 1000–2000 varieties of candles [1]. Because of their common use, this study focuses primarily on paraffin wax candles of the taper variety, with a single column-type candle investigated for comparative purposes. Early in the investigation, it was found that the burning rate and heat flux from the candle flame depends on many interdependent factors including wick length, wick shape, mass burning rate, heat release rate, flame height, and paraffin wax formulation, which has a direct effect on the density, melting point, and viscosity. Therefore, taper-type candles became the primary focus of this preliminary burning characterization and heat flux study (see Figure 1).

The primary candle selected for the study was a 305-mm long white, paraffin wax, taper-style candle with a diameter of 21 ± 0.5 mm over its entire length. The wick was a flat braid type, approximately 1 mm \times 2 mm wide.

PARAFFIN WAX

The primary component of a candle is paraffin wax, which is a composite material that is made up of a mixture of straight-chain hydrocarbon molecules. The molecular formula for paraffin is C_nH_{2n+2} , where the value of n ranges from 19 to 36 and the average value is 25 [8].

The characteristics of a particular paraffin wax are commonly defined by its physical properties. These properties include melting point, penetration, drop point, viscosity, oil content, color, odor, and others listed in Table 1. These properties help manufacturers assess the appropriateness of a particular wax for a particular type of candle that they intend to manufacture. The most important of these properties from a manufacturing standpoint is the melting point, which dictates the type of candle that can be produced. For instance, the melting point of the paraffin wax used in the

Table 1. Properties of paraffin candle wax from the literature.

| Property | Value | Reference |
|--|----------------------------|-----------------|
| Carbon number, range (C_nH_{2n+2}) | 19–36 | [8,10] |
| Carbon number, average (C_nH_{2n+2}) | 23–25 | [8] |
| Molecular weight (average) | 350–420 kg/kmol | [8] |
| Melting point | 48–68°C | [8,10,11,13,14] |
| Congeaing point | 66–69°C | [12,13] |
| Flash point | 204–271°C | [8,10,11,13] |
| Fire point | 238–263°C | [14] |
| Boiling point | 350–430°C | [12] |
| Oil content (average) | 0.1–0.5% | [13,14] |
| Oil content (maximum) | 0.5–0.9% | [13] |
| Density (at room temperature) | 865–913 kg/m ³ | [12,15] |
| Density (at 82°C) | 766–770 kg/m ³ | [16] |
| Specific gravity | 0.82–0.92 | [11] |
| Kinematic viscosity (at 100°C) | 3.1–7.1 mm ² /s | [10,13,14] |
| Vapor pressure (at 100°C) | 2.67 kPa | [11] |
| Net heat of combustion | 43.1 MJ/kg | [17] |
| Gross heat of combustion | 46.2 MJ/kg | [17] |
| Latent heat of fusion | 0.147–0.163 kJ/g | [12] |
| Specific heat (solid at 35–40°C) | 2.604 kJ/kg K | [12] |
| Specific heat (liquid at 60–63°C) | 2.981 kJ/kg K | [12] |
| Thermal conductivity (at room temperature) | 0.23 W/m K | [15] |
| Melted wax temperature (average, around base of wick) | 82–85°C | [18,19] |
| Maximum flame temperature | 1400°C | [20] |

manufacture of taper and pillar candles ranges from 59 to 65°C [9]. Heat release properties, such as the effective heat of combustion are not of interest to wax producers or candle manufactures and are therefore typically not measured. A list of material properties for paraffin wax has been provided in Table 1. The properties presented represent ranges of values and due to the incompleteness of data from each reference, only limited attempts have been made to relate the dependence of these properties, i.e., the melting point with respect to flash point, density, and kinematic viscosity as presented in Figures 2–4.

The heat release rate of the candle has a direct impact on the character of a candle including its heat flux distribution. In order to develop an accurate understanding of the behavior of a candle, the heat of combustion of the burning wax is important. As Table 1 indicates, only one value for the net heat of combustion could be found in the literature [17]. Measurements of the heat of combustion of the candle using the cone calorimeter and an oxygen bomb calorimeter are described next.

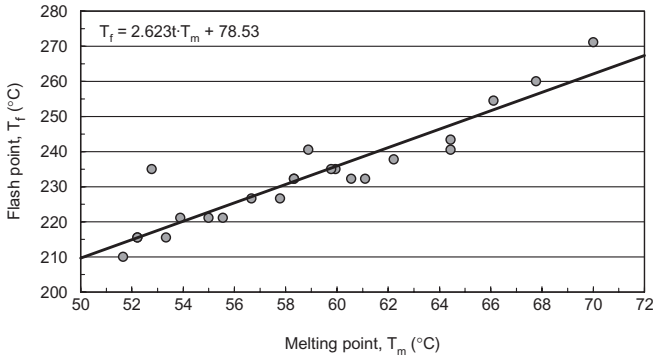


Figure 2. Temperature dependence of the flashpoint of paraffin candle wax [8,10,11,13].

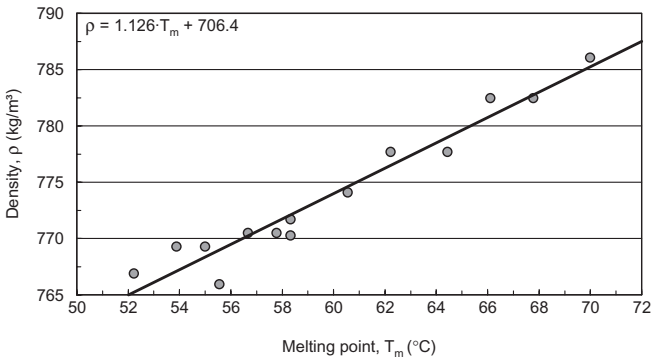


Figure 3. Temperature dependence of the density of paraffin candle wax [13,16].

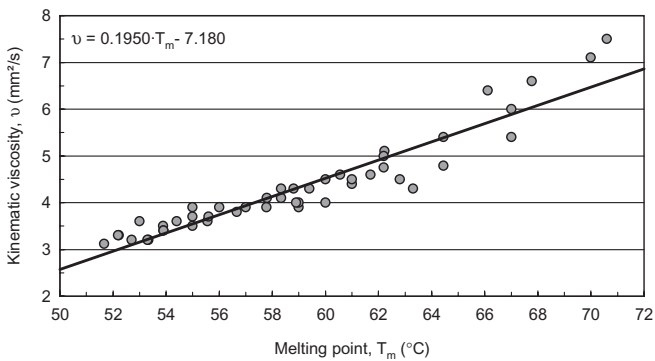


Figure 4. Temperature dependence of the kinematic viscosity of paraffin candle wax [10,11,14].

The effective heat release rate (\dot{Q}) of a burning candle flame is the product of the mass burning rate of the fuel (\dot{m}), the net heat of complete combustion of the fuel (H_c), and the combustion efficiency (χ_a):

$$\dot{Q} = \chi_a \cdot \dot{m} \cdot H_c \quad (1)$$

where the product of χ_a and H_c is the effective heat of combustion ($\Delta h_{c,\text{eff}}$):

$$\Delta h_{c,\text{eff}} = \chi_a \cdot H_c \quad (2)$$

In general, the combustion efficiency varies for different fuels, and is limited by definition to values between 0 and 1. For the paraffin wax studied here, χ_a was determined by several ways as described here.

In addition to the mass burning rate and the heat of combustion, the radiative heat loss fraction also influences flame behavior. The radiative fraction (χ_r) characterizes the importance of radiative emission from a fire or flame. It is defined as the ratio of the rate of radiative energy emitted to the surroundings (\dot{Q}_r) to the heat release rate ($\dot{m} \cdot H_c$):

$$\chi_r = \frac{\dot{Q}_r}{\dot{m} \cdot H_c} \quad (3)$$

To determine χ_r , the values of \dot{Q}_r , \dot{m} , and H_c were measured for the candle as described as follows.

EXPERIMENTAL APPARATUS AND PROCEDURE

Heat of Combustion

The effective heat of combustion ($\Delta h_{c,\text{eff}}$) for the paraffin wax samples selected for study were determined using the cone calorimeter in accordance with ASTM E 1354 [21]. In an independent set of experiments, the net heat of combustion (H_c) was determined using an isoperibol oxygen bomb calorimeter in accordance with ASTM D5865-03a [22]. Equation (2) relates the effective heat of combustion ($\Delta h_{c,\text{eff}}$) to the net heat of combustion (H_c).

The candles were broken into small pieces and the wick material was removed. For the cone calorimeter experiments, test specimens were prepared by placing the wax pieces into a 8-mm thick by 75-mm diameter mold. A press maintained at an elevated temperature and pressure (45°C and 28 MPa) was used to produce the uniform test specimens shown in Figure 1. A number of experiments were conducted with the cone heater set

to incident heat fluxes from 10 to 40 kW/m². For analysis of the cone data, the heat of combustion per gram of oxygen ($\Delta h_c/r_o$) was taken as 12.7 ± 0.1 MJ/kg, consistent with other species with molecular formula C_nH_{2n+2} , or equivalently 43.8 ± 0.7 MJ/kg of fuel. The effective heat of combustion for each test specimen was calculated over the time period from ignition of the specimen to the time when the flame was out. For the oxygen bomb calorimeter, small (≈ 0.5 g) wax samples cut from the candles were used for testing.

Candle Flames

Experiments were conducted in a $0.61 \times 0.61 \times 0.76$ m³ (width \times length \times height) enclosure to reduce drafts and facilitate establishment of a laminar candle flame. The chamber was raised 20 mm off the supporting surface, and the bottom surface was provided with 44 uniformly spaced 6-mm diameter holes around the perimeter to allow fresh air to enter the chamber without producing unwanted drafts. A 150-mm diameter hole fitted with a 150-mm high chimney was provided at the top of the chamber to allow heat and combustion products to vent into an exhaust hood. One side of the chamber was hinged and provided with two latches to allow access to the inside of the chamber for specimen placement, ignition, and platform adjustment during the experiments. The candles were supported in the vertical orientation on a load cell within the chamber (see Figure 5). The load cell was located

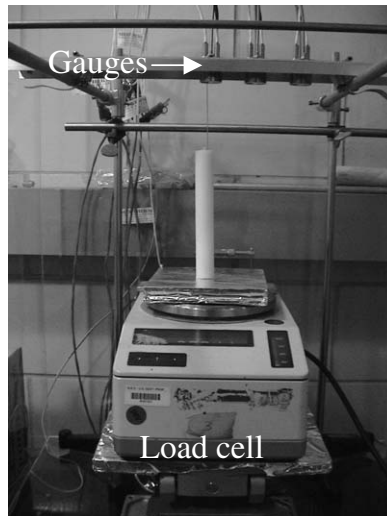


Figure 5. Candle on load cell.

on a jack stand that allowed the entire assembly to be raised or lowered during a test in the vertical direction. The Schmidt–Boelter heat flux transducers were mounted in a rigid frame either horizontally above the candle specimen as shown in Figure 5 or in a vertical orientation for measurement of the radial flux. The transducers were water cooled with a 25-mm diameter copper body. Each transducer contained one 9.5 mm diameter total heat flux sensor as well as one 7.5 mm diameter radiant heat flux sensor located 13 mm apart. For measurements in the flame and near the flame tip, a Schmidt–Boelter total heat flux gauge with a diameter of 3.2 mm was used to reduce the impact of the gauge on the flame structure. The Schmidt–Boelter flux gauges were calibrated water-cooled thermopiles, whose sensor surface temperature was uniform and similar to that of the cooling water. This makes it preferable over flux gauges of the Gardon design (metal foil sensor with a single central thermocouple) for measurements involving mixed convective and radiative heat fluxes. The Schmidt–Boelter gauges have a nominal field of view of 180° and a time response of ≈ 0.5 s. A type K thermocouple was positioned in the water flow exiting the transducers to ensure that the flux from the candle flame did not produce a temperature increase in the transducer. The water supplied to the transducers was heated to $77 \pm 2^\circ\text{C}$ in order to eliminate condensation on the surface of the transducers. The elevated temperature of the cooling water was found to impact the zero-flux signal offset, but not the value of the calibration itself. Additional thermocouples were positioned at the top and bottom of the chamber to monitor the ambient conditions. The voltage output of the transducers and thermocouples was recorded digitally by a data acquisition system every 3–5 s.

The radiant heat flux sensor on the dual gauges was fitted with a sapphire window to prevent convective heating. The manufacturer's calibration was used. The sources of uncertainty in the measurement were uncertainty in the voltage reading and uncertainty in the calibration. The dominant uncertainty with this type of gauge was the calibration itself. Sapphire cuts off at $\approx 6.5 \mu\text{m}$ [23] and the manufacturer calibration accounts for this. A comparison of the Schmidt–Boelter flux gauge and the radiant heat flux sensor at locations where the convective flux was considered negligible confirmed that the calibrations were consistent with each other in a convection-free environment.

A recent round-robin test [24] of similar gauges at five international fire facilities (using a variety of calibration methods) indicated a standard deviation of about $\pm 3\%$, or $\pm 3 \text{ kW/m}^2$ at a flux of 100 kW/m^2 . In the round-robin study, the calibration by the manufacturer of this gauge fell well within the range of variation of the other lab-to-lab variations. Thus, the same calibration uncertainty ($\pm 3\%$) was applied here.

Prior to each test, the position of the candle in relation to the heat flux gauges was verified. This was often difficult, but could be simplified by conducting each test with a candle that had been pre-burned for 20–30 min and allowed to cool. Burning the candle allowed the natural curvature of the wick to become obvious, which then allowed the position of the candle flame to be more accurate since it was recognized that the tip of the flame was generally centered above the center of the curved wick. If an unburned candle were positioned based on the center of the wick, the direction of curvature could move the flame, changing the relative position of the sensor to the flame and thereby reducing the accuracy of the flux measurements.

A digital camera was mounted on an adjustable stand just outside the wall of the test chamber. Close-up digital photographs of the top portion of the burning candle were taken approximately every 1–2 min over the entire test duration. The photographs were used to determine the flame and wick heights as well as the height of the candle with respect to time. A metal ruler with 1 mm graduations was positioned directly next to the candle, which allowed measurements to be made based on physical comparison.

Most tests were conducted for several hours in order to obtain representative sampling of heat flux measurements with respect to the relative height of the flame. The overall distance between the candle and the heat flux transducers was adjusted by lowering or sometimes raising the platform of the jack stand. An additional metal ruler was positioned vertically next to the stand to allow the platform height to be adjusted to within ± 0.5 mm.

EXPERIMENTAL RESULTS

Heat of Combustion

The average ($n=5$) gross heat of combustion ($\Delta h_{c,\text{gross}}$) was measured in accordance with ASTM D5865-03a [22] as 46.5 kJ/g with a standard deviation of 0.3 kJ/g. The net heat of combustion (H_c) and the standard uncertainty was calculated using a hydrogen mass fraction of 0.1477 for paraffin, yielding $H_c = 43.3 \pm 0.3$ kJ/g, which overlapped the cone results and the literature value within experimental uncertainty. It should be noted that this estimate was for the paraffin wax only and does not take into account combustion of the wick. The contribution of the wick to the heat of combustion, however, was assumed to be relatively small, as the mass fraction of the wick was less than 0.1% of the wax–wick system.

The average effective heat of combustion ($\Delta h_{c,\text{eff}}$) of the primary test candle was determined for incident heat flux exposures of 10–40 kW/m² in the cone calorimeter [21]. The measured peak heat release rate per unit

sample surface area ranged from 800 to 4150 kW/m² (for incident fluxes of 10 and 40 kW/m², respectively). The $\Delta h_{c,\text{eff}}$ was found to be relatively insensitive to incident heat flux. The average value of the measured $\Delta h_{c,\text{eff}}$ for the paraffin wax at the various flux levels was measured as 43.8 ± 0.7 kJ/g. The value of $\Delta h_{c,\text{eff}}$ was also measured for candles with eight different wax formulations at an incident flux of 10 kW/m². This flux level was found to provide a steady burning rate. The $\Delta h_{c,\text{eff}}$ for the eight different wax formulations tested was found to be highly similar with an average value of 43.7 kJ/g and a standard deviation of 0.6 kJ/g ($\approx 1\%$). The combustion efficiency, using Equation (2) and an H_c from the bomb calorimeter of 43.3 ± 0.3 kJ/g was, therefore, nearly complete.

An estimate of the combustion efficiency was also attained by examining the products of incomplete combustion from the cone calorimeter data. The combustion efficiency was defined as the ratio of the net heat of incomplete combustion to the net heat of complete combustion. The standard heats of formation and the measured mass yields of CO, CO₂, and soot were used to calculate the net heat of incomplete combustion. For irradiance levels of 10–40 kW/m², the measurement of the CO yield in the cone varied from 0.006 to 0.014 g/g, and the soot yield varied from 0.035 to 0.045 g/g. The total hydrocarbon yield was assumed to be less than 0.005 g/g. Assuming a stoichiometry for the paraffin wax of C₂₄H₅₀, the combustion efficiency was found to vary from 0.96 to 0.97. Other appropriate stoichiometries led to nearly identical results. The resulting combustion efficiency was consistent with the value found from the measured heat release rate. The results suggest that combustion was nearly complete, which is reasonable for candle flames that do not visibly emit soot, as observed in this study.

Candle Flames

The mass burning rate (expressed as the mass loss rate), candle regression rate, and flame height are expressed graphically in Figures 6–8, respectively. The flame height, h_f , is defined as the relative distance between the visible flame tip and the wax pool surface. Each graph represents data obtained from a number of independent tests (either 3 or 5, as indicated). The purpose of these measurements was to characterize the burning behavior of the candles. As the figures indicate, it took 12–15 min to obtain steady burning behavior, after which there was very little change. The time to reach steady state was measured to be about 5 min shorter for pre-burned candles, probably due to the existence of a pre-formed cup, the structure that enfolds the molten pool of wax. Data correlations representing the measured mass loss rate, regression rate, and flame height as a function of

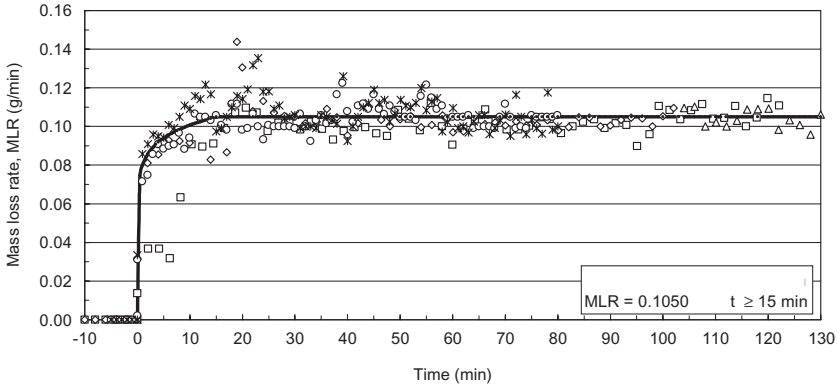


Figure 6. Mass loss rate of a 21-mm diameter candle as a function of time after ignition ($n = 5$ tests).

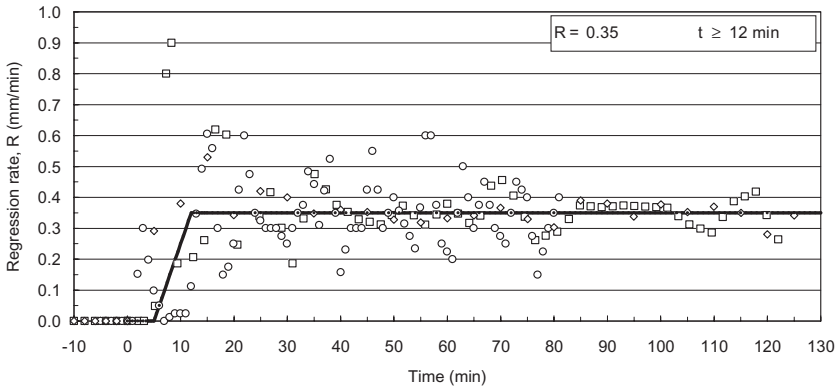


Figure 7. Regression rate of a 21-mm diameter candle as a function of time after ignition ($n = 3$ tests).

time after ignition (at time zero) are shown in the figures. The relative standard uncertainty ($1 \cdot \sigma$) in the measurements was estimated as 12, 18, and 9% for the mass loss rate, the candle regression rate, and the flame height, respectively, based on the repeat measurements. The regression rate (R) is related to the mass loss rate (\dot{m}) as:

$$R = \frac{\dot{m}}{\frac{1}{4}\pi D^2 \cdot \rho} \quad (4)$$

where ρ is the density of the candle, and D is its diameter. The density was determined through measurement of the mass using a load cell, and

an estimate of the volume (with $D = 21$ mm), which yielded a value of 847.0 kg/m^3 . This density was slightly (about 2%) smaller than values reported in the literature (see Figure 3 and Table 1). From the measured mean mass loss rate shown in Figure 6 ($\dot{m} = 0.105 \text{ g/min}$), Equation (4) shows that $R = 3.6 \text{ mm/min}$, which is within 3% of the measured value shown in Figure 7.

From measurements of the mean mass loss rate (0.105 g/min) and $\Delta h_{c,\text{eff}}$ (43.8 kJ/g), the steady-state heat release rate from the candle was calculated as $77 \pm 9 \text{ W}$. The mean flame height was measured as $42 \pm 1 \text{ mm}$. Measurements of the total and radiative heat flux from the candle flames were made in both the horizontal and vertical directions at varying radial distances from the center of the flame. The radiative heat flux is discussed in the context of CFD modeling in the next section.

The heat flux measurements as a function of radial location at two heights above the base of the flame are presented in Figure 9. It was observed that once steady burning had been established, the base of the flame was consistent with the top lip of the solid candle within 1–2 mm. Figure 9 shows the total flux above the flame tip measured by the 3 mm diameter sensor. The large diameter heat flux transducers could only be brought to within $\approx 50 \text{ mm}$ of the top of the candle before the flame structure was noticeably impacted. At closer distances, the presence of the heat flux transducer significantly affected the behavior of the flame (e.g., the height). The smaller gauge (3 mm diameter) did not significantly affect the flame when it was within 20 mm of the flame tip. The standard ($1 \cdot \sigma$) combined relative uncertainty for the heat flux was estimated as 8% on the centerline and 6% off-centerline based on repeat measurements and a propagation of error analysis. The uncertainty was higher above the centerline due to the

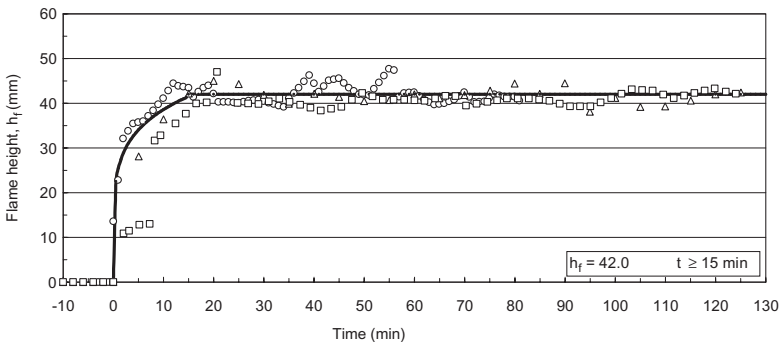


Figure 8. Flame height of a 21-mm diameter candle as a function of time after ignition ($n = 3$ tests).

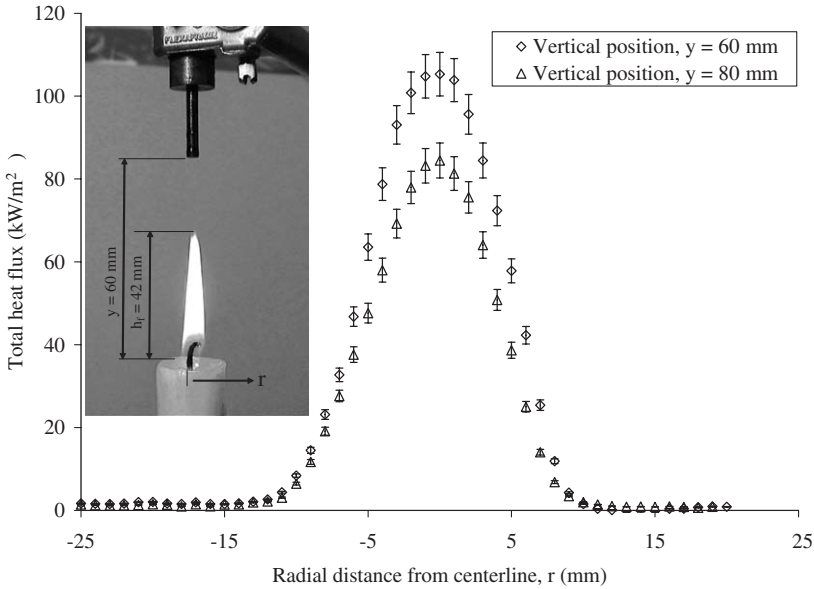


Figure 9. Heat flux above the flame as a function of radial distance from the flame centerline at two vertical positions above the base of the candle using a 3-mm diameter total heat flux gauge.

relatively larger scatter in the data. The highest measured flux was about 145 kW/m^2 , which was measured at the flame tip. The flux decreased with distance from the candle, obtaining values of 105 and 90 kW/m^2 , 18 and 38 mm above the tip (see Figure 9). At locations 260 mm above the candle base, the average flux was on the order of only 10 kW/m^2 and large fluctuations in the measurements were observed, which were directly attributed to the turbulent disturbance of the buoyant plume. Figure 9 also shows that the heat flux in the axial direction at radial distances greater than 13 mm and heights 60 mm above the candle base was relatively small. The candle flame was not exactly symmetric about the center of the candle base. Indeed, the wick was curved, and the flame tip was not precisely above the candle center. Figure 9 substantiates this, as the flux was slightly larger on the side closer to the top of the wick, that is, the side at which the wick was pointing.

Figure 10 shows the measured total and radiative heat flux as a function of height above the base of the flame for a gauge positioned at a radial distance 11 mm from the flame centerline and with the gauge directed toward the centerline (see inset in figure). The peak flux at this radial location was more than an order of magnitude smaller than the heat flux

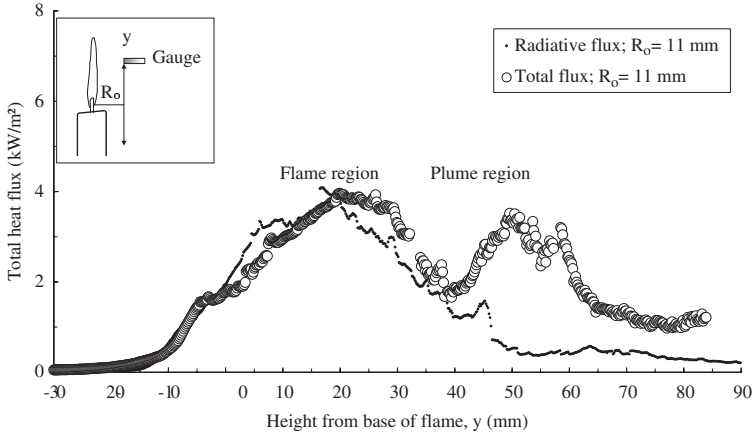


Figure 10. Total and radiative heat flux as a function of height above the base of the flame at a radial distance 11 mm from the flame centerline. The expanded uncertainty in the total and radiative heat flux is 12%.

directly above the center of the candle flame, as seen in Figure 9. It should also be noted that the radiative flux onto the gauge was undoubtedly affected by the view factor and gauge orientation for such close locations to the flame. It is evident in Figure 10 that the radiative heat flux was the predominant form of heat transfer over the length of the visible flame, that is, over the first 40 mm above the base of the flame. The label in Figure 10 refers to this zone as the *flame region*. For locations above this zone, radiative heat flux was less significant and convective heat transfer apparently dominates, presumably due to the plume of hot combustion products exiting the candle flame. In this context, consideration of Figure 9 suggests that the physical width of the hot plume, 60 and 80 mm above the base of the candle, was on the order of 25 mm in diameter. The flux profiles (in Figure 9) also suggest that the plume was fairly straight, with a shape not unlike a cylinder, at least from 60 to 80 mm above the candle. An additional series of radial heat flux measurements (similar to those shown in Figure 10) at a height of 50 mm above the base of the flame confirmed the data presented in Figure 10. For distances farther from the candle (radial distances greater than 15 mm), the total and radiative heat fluxes became nearly equal.

The radiative emission by the candle flame to the surroundings was determined by integrating the radiative heat flux shown in Figure 10 along the y -axis, representative of a control volume surrounding the candle. Assuming axisymmetry, the radiative heat flux data, $\dot{q}_r'' (R_o = 11 \text{ mm}, y)$,

in Figure 10 was integrated in the vertical (y) direction to determine the approximate value of \dot{Q}_r following [25]:

$$\dot{Q}_r = \pi R_o^2 \int_{-\infty}^{\infty} \dot{q}_r''(y) dy \quad (5)$$

where $R_o = 11$ mm.

The radiative fraction emitted to the surroundings was determined using Equation (3). The total heat release rate of the flame was taken as the product of the average mass loss rate and the measured net heat of combustion (H_c). The radiative fraction was determined by finding the ratio of the radiative emission and $\dot{m} \cdot H_c$, which yielded a value of 0.17 ± 0.01 . A propagation of error analysis for the radiative fraction measurement considering uncertainty in both the mass burning rate and the radiative flux measurements showed that the dominant contributor to the uncertainty in the radiative fraction was uncertainty in the radiometer calibration.

CFD MODELING

In order to determine heat flux exposures from candle flames at different positions and the reaction of target materials, the candle flame was modeled using the NIST Fire Dynamics Simulator (FDS) [26]. This FDS is a computational fluid dynamic (CFD) fire model that predicts and visualizes the spread, growth, and suppression of a fire based on the underlying scientific principles governing fluid motion. The model numerically solves the conservation equations of mass, momentum, and energy that govern low-speed, thermally driven flows with an emphasis on smoke and heat transport from fires. Throughout its development, FDS has been aimed at solving practical fire problems in fire protection engineering, while at the same time providing a tool to study fundamental fire dynamics and combustion. So, FDS has been used successfully to model laminar flames [27].

In this study, the simulation of heat flux was emphasized in an effort to develop a tool that could be used in arson investigation. A companion software package, called Smokeview, graphically presents the results of the FDS three-dimensional time-dependent simulation as it animates the flame structure in three dimensions including the heat flux, temperature, and fluid velocity field [26]. The FDS/Smokeview software package allows viewing of the simulated results from any angle and from inside or outside the computational boundaries.

The core hydrodynamic algorithm is an explicit predictor–corrector scheme, second order accurate in space and time. The FDS uses a mixture fraction combustion model. The mixture fraction is a conserved scalar

quantity that is defined as the fraction of gas at a given point in the flow field that originated as fuel. This model assumes that combustion is mixing-controlled, and that the reaction of fuel and oxygen is infinitely fast. The mass fractions of all of the major reactants and products can be derived from the mixture fraction by means of 'state relations,' empirical expressions arrived at by a combination of simplified analysis, and measurement. Radiative heat transfer is included in the model via the solution of the radiation transport equation for a non-scattering gray gas. This equation is solved using a technique similar to finite volume methods for convective transport, thus it is known as the finite volume method (FVM). Approximately 100 discrete angles are used to determine the distribution of radiative energy at each point. Thus, FDS approximates the governing equations on a rectilinear grid. All solid candle surfaces were assigned thermal boundary conditions in addition to information about the burning behavior of the material. For application to candle flames, FDS needs experimental data to guide model development, and to ascertain the accuracy of the model predictions. The simulation results were evaluated based on accurate visual depiction of the flame shape and height, and comparison of the calculated and measured flux directly above the flame tip.

Model input parameters were adjusted to meet these two criteria better and once they were sufficiently met, the additional output parameters were evaluated and compared with the experimental values. For the initial modeling simulations, a $48 \times 48 \times 80 \text{ mm}^3$ (length \times width \times height) domain was created around the virtual candle. The grid size was $1 \times 1 \times 2 \text{ mm}^3$ around the candle and expanded to $2 \times 2 \times 2 \text{ mm}^3$ near the edges of the domain using the FDS linear grid transformation algorithm. This resulted in a total of 51,840 cells. For some cases, the height of the domain was extended, leading to a significantly larger number of cells and more lengthy computational run times. The wax portion of the candle was modeled as a solid inert material. The geometry of the candle including the circular shape and the curved wax pool were represented in as detailed a manner as the grid allowed. This was done to provide a realistic boundary condition for the flow of air into the flame. Preliminary models using a simple square shape produced noticeable effects on the airflow to the flame and on the heat flux to the surfaces above the flame. The boundary conditions for the flame model accounted for the presence of the heat flux gauge itself, which impacted the flow field.

The curvature of the wick was approximated from photographs. The wick was modeled as a 1-mm diameter cylinder that was 12 mm tall, with curvature causing it to extend 5 mm from the centerline in the radial direction. The lower 4 mm of the wick was taken as non-burning, which was consistent with observations that showed that the base of the flame was

about 4 mm above the molten wax pool. The heat release per unit area from all surfaces of the wick was taken as a uniform value of 1967 kW/m^2 . This heat release rate was based on the average measured mass burning rate of the candle (0.105 g/min), the heat of combustion value measured in cone calorimeter experiments (43.8 kJ/g), and the surface area of the burning wick (39 mm^2).

The calculations required information on the stoichiometry of the fuels and the radiative fraction of the flame. The properties of the burning wax were based on $\text{C}_{24}\text{H}_{50}$, which is a reasonable approximation, as seen in Table 1. To test the sensitivity of the result to fuel properties, calculations were also performed using the properties of *n*-heptane (C_7H_{16}) and methane (CH_4). The stoichiometry was defined by the molecular composition. The calculated heat flux was sensitive to the input radiative fraction, which was taken as 17%, as measured.

Figure 11 compares a photo-image of a burning candle to the simulated flame represented by the isosurface of stoichiometric mixture fraction, which provides an adequate representation of the flame shape. The calculated flame height is 40 mm as compared to the measured value of 42 mm. Figure 12 compares the simulated vertical and horizontal heat flux

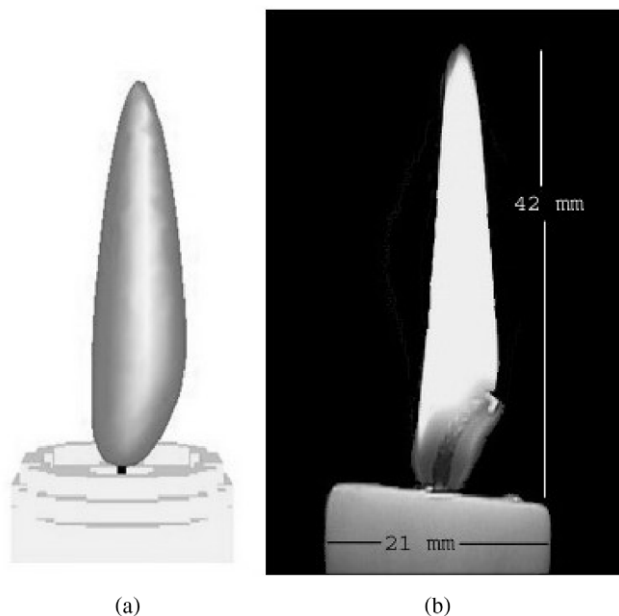


Figure 11. (a) Simulation of the burning candle as represented by the calculated isosurface of stoichiometric mixture fraction and (b) photograph of the burning 21-mm diameter candle.

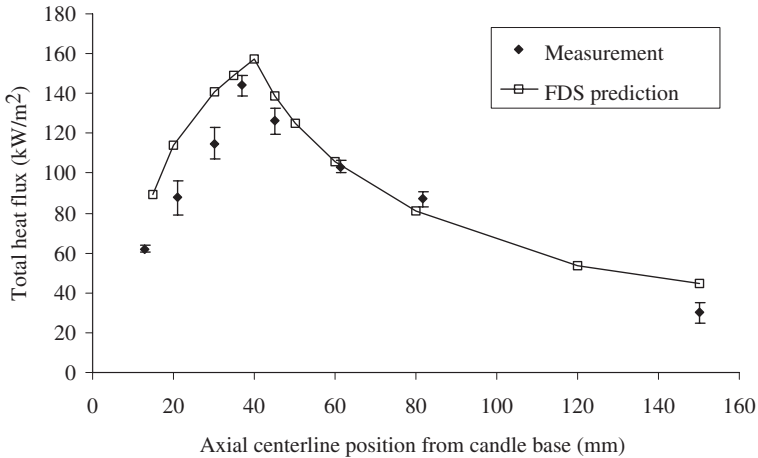


Figure 12. Total heat flux in the upward direction as a function of distance above the candle base along the centerline.

values predicted by FDS with the experimental measurements. The results in Figure 12 show a measured and simulated peak heat flux near the flame tip of 145 and 160 kW/m², respectively. The error bars in the figure represent the standard deviation based on repeat measurements. The measurements agree reasonably well with the FDS simulation results.

CONCLUSIONS

Fires caused by candles are occurring at an increasing rate every year. Despite this fact, there is a lack of available information that fire investigators can use to help determine the potential of a candle to ignite adjacent fuels. Through this study, an attempt has been made to bridge this gap and build a modeling tool that can be used by fire investigators. In the initial part of this study, the basic properties of paraffin wax have been compiled, measurements and data on the burning characteristics of paraffin wax candle have been presented. The input parameters necessary to model that candle flame have been provided, along with a comparison of predicted and measured values. The results of the model validation provide input procedures and properties necessary to model candle flames of different geometries as well as the interaction of those flames with different targets, ultimately facilitating insight into the possibility of ignition.

Given enough time, the heat flux generated by a typical candle is large enough to ignite secondary objects located even 200 mm above the base of the candle. Nearby objects that are not directly over the candle base can also

be ignited, but must be located much closer for ignition to occur. The development and validation of a computer simulation of a candle flame may provide a tool for arson investigators as they attempt to test ignition hypotheses.

Additional research is needed on the topic of candle burning. Information provided by the CPSC [2] indicates that many candle-related fires are due to causes other than unattended candles, close proximity to combustibles, or negligence. These include candle flare-up, candles that explode, low wax level, shattered containers, flammable containers, candle reignition, and tip-over. These types of events clearly need further investigation. In addition, the ignition of real materials by candles needs to be investigated. In this regard, experiments investigating the ignition of representative materials exposed to candle flames in various orientations would be of value to arson investigators.

ACKNOWLEDGMENTS

This work was funded by the National Institute of Justice through the Office of Law Enforcement Standards. The authors are grateful to Michael Smith of NIST, who carefully performed the cone calorimeter measurements and to Susan Ballou who was the scientific monitor of this work for the Office of Law Enforcement Standards at NIST.

REFERENCES

1. "The Candle Industry," National Candle Association, Washington, DC, 2002.
2. Kyle, Susan, "Preliminary Report on In-Depth Investigations of Incidents Involving Candle," Consumer Product Safety Commission, March 2002.
3. Ahrens, M., "Home Candle Fires," National Fire Protection Association, September 2004.
4. Candle Fires in Residential Structures, Topical Fire Research Series, Vol. 12, No. 12, U.S. Fire Administration, Emmitsburg, MD, February 2001 (Revised December 2001).
5. "Candle Use and Safety," National Candle Association, Washington, DC, 2002.
6. Faraday, M., Faraday's Chemical History of a Candle, Chicago Review Press, Chicago, IL, 1988, 124 pp.
7. "Candle Making and Ingredients," National Candle Association, Washington, DC, 2002.
8. Kirk-Othmer, Encyclopedia of Chemical Technology, Third Edition, Vol. 24, John Wiley & Sons, New York, pp. 473-476.
9. "Wax Product List - Petroleum & Natural Wax Products," Hase Petroleum Wax Company, Arlington Heights, IL, 2002.
10. Technical Bulletin - Shell Paraffin and Microcrystalline Waxes: SHELLWAX[®] and SHELLMAX[®], Shell Lubricants, October 2000.

11. Material Safety Data Sheets (MSDS) for Paraffin Wax.
12. North American Combustion Handbook, Second Edition, North American Mfg. Co., Cleveland, OH, p. 362.
13. Product Information Bulletin DG-4A – Fully Refined Paraffin Waxes, Exxon Mobil Corporation, August 13, 1999.
14. “Paraffin Waxes,” Asheville Oil Company, 2002.
15. “Properties of Non-Metallic Solids,” Wattage Calculation Formulas – Paraffin Melting, Hotwatt Inc., Danvers, MA, Heaters for Every Application website, www.hotwatt.com
16. “Chevron Refined Waxes,” Chevron Lubricants, 2002.
17. Cote, A.E. and Linville, J., eds., Fire Protection Handbook, Seventeenth Edition, National Fire Protection Association, Quincy, MA, 1991.
18. Sanderson, Jack, “Candle Fires,” Fire Findings, Vol. 5, No. 4, Fall 1997, pp. 7–11.
19. Townsend, David, “Fires Associated with the Use of Night Light Candles (Tea Lights),” London Fire Brigade, October 1999.
20. Gaydon, A.G. and Wolfhard, H.G., *Flames: Their Structure, Radiation and Temperature*, Fourth Edition, John Wiley and Sons, Inc., New York, 1979, 460 p.
21. ASTM E 1354-99, “Standard Test Method for Heat and Visible Smoke Release Rates for Materials and Products Using an Oxygen Consumption Calorimeter,” ASTM International, West Conshohocken, Pennsylvania, 1999.
22. ASTM D5865-03a, “Standard Test Method for Gross Calorific Value of Coal and Coke ASTM International,” West Conshohocken, Pennsylvania, 1999.
23. Wolfe, W.L. and Zissis, G.J., eds., *The Infrared Handbook*, Office of Naval Research, Dept. of the Navy, Washington, D.C., 1978.
24. Pitts, W.M., Murthy, A.V., de Ris, J.L., Filtz, J.-R., Nyård, D., Smith, D. and Wetterlund, I., “Round Robin Study of Total Heat Flux Gauge Calibration,” NIST Special Publication 1031, National Institute of Standards and Technology, Gaithersburg, MD, October 2004.
25. Hamins, A., Klassen, M., Gore, J. and Kashiwagi, T., “Estimate of Flame Radiance via a Single Location Measurement in Liquid Pool Fires,” *Combustion and Flame*, Vol. 86, 1991, pp. 223–228.
26. McGrattan, K.B. (ed.), Baum, H.R., Rehm, R.G., Forney, G.P., Floyd, J.E., Prasad, K. and Hostikka, S., *Fire Dynamics Simulator (Version 3), Technical Reference Guide*, NISTIR 6783, National Institute of Standards and Technology, Gaithersburg, MD, November 2002.
27. Mukhopadhyay, A. and Puri, I., “An Assessment of Stretch Effects on Flame Tip Using the Thin Flame and Thick Formulations,” *Combustion and Flame*, Vol. 133, 2003, pp. 499–502.
28. Forney, G.P. and McGrattan, K.B., *User’s Guide for Smokeview Version 4*, Technical Report NIST Special Publication 1017, National Institute of Standards and Technology, Gaithersburg, Maryland, June 2004.